The progression of infiltrating neurovascular features and chemokine production of the caudal intervertebral disc following injury

Remy E. Walk[1], Kaitlyn S. Broz[2], Liufang Jing[1], Ryan P. Potter[3], Alec T. Beeve[1,4], Erica L. Scheller[1,4], Munish C. Gupta[5], Lori A. Setton[1,3,5], Simon Y. Tang[1-3,5]

[1]Department of Biomedical Engineering, Washington University in St. Louis, St. Louis, MO
[2]Institute of Material Science and Engineering, Washington University in St. Louis, St. Louis, MO
[3]Department of Mechanical Engineering and Materials Science, Washington University in St. Louis, St. Louis, MO
[4]Department of Medicine, Washington University School of Medicine, St. Louis, MO
[5]Department of Orthopaedic Surgery, Washington University School of Medicine, St. Louis, MO

Corresponding Author:
Simon Y. Tang, Ph.D., MSCI
Associate Professor
Orthopedic Surgery, Biomedical Engineering,
Mechanical Engineering & Materials Science
Washington University in St. Louis
simon.tang@wustl.edu

Keywords: intervertebral disc degeneration; inflammatory chemokines; intradiscal vascularization; innervation; low back pain pathoanatomy

Abstract

The accessibility of the mouse caudal intervertebral disc (IVD) and its geometric semblance to the human IVD makes it an attractive model for assessing IVD-specific responses *in vivo*. To effectively utilize this model, the temporal trajectories of key pathoanatomical features, such as the production of inflammatory chemokines, tissue disorganization, and neo- vessel and neurite infiltration, must be understood. This study aims to define the progression of chemokine production and neurovascular invasion at 2-, 4-, and 12-weeks following a caudal IVD injury in 3-month-old female C57BL6/J mice. We measured IVD-secreted chemokines and matrix metalloproteinases (MMPs) using multiplex ELISA, graded the histopathological degeneration, and quantified the intradiscal infiltrating vessels (endomucin) and nerves (protein-gene-product 9.5) using immunohistochemistry. Injury provoked the secretion of IL6, CCL2, CCL12, CCL17, CCL20, CCL21, CCL22, CXCL2 and MMP2 proteins. Neurites propagated rapidly within 2-weeks post-injury and remained relatively constant until 12-weeks. Peak vascular vessel length occurred at 4-weeks post-injury and regressed by 12-weeks. These findings identified the temporal flux of inflammatory chemokines and pain-associated pathoanatomy in a model of IVD degeneration using the mouse caudal spine.

1. Introduction

Low back pain affects up to 85% of the population worldwide[1,2], and intervertebral disc (IVD) degeneration is a significant contributing factor.[3] The IVD is a cartilaginous soft tissue and is considered avascular and aneural.[4] The functional spinal unit consists of the IVD and adjacent vertebral bodies where the IVD provides resistance against compressive loads and shock absorbance for the musculoskeletal system. With degeneration, the IVD has compromised ability to perform these essential functions and can become painful.[3] Some key hallmarks of IVD degeneration include disorganization of the IVD tissue, secretion of inflammatory chemokines and growth factors[5,6], and infiltration of blood vessels and nerves.[7,8]

In addition to the structural collapse and the depletion of proteoglycan-rich matrix, other biological features in the degenerating IVD may be culprits to chronic pain, including the production of inflammatory chemokines, expression of catabolic enzymes, and the invasion of neurites and vessels.[9,10] Chemokines canonically recruit immune cells, which in turn secrete more chemokines that further exacerbate the inflammatory state of the degenerating IVD[11], and the immune cells can further accelerate the breakdown of the extracellular matrix.[12,13] Chemokines produced by the IVD may also contribute to neuron and vessel propagation around and into the outer annulus fibrosus which may mediate of IVD degeneration associated low back pain.[14]

Animal models are a common tool for studying IVD degeneration. Injury such as via mechanical overload[15–18] and needle puncture[19–33] are used to induce degeneration of the IVD. Though the lumbar spine is more clinically relevant as a site of pain generation compared to the caudal spine, the surgical exposure required to access the lumbar IVD is traumatic, and the surrounding inflammation may confound the IVD-specific responses. Puncture injury to the caudal IVD does not require surgical exposure and can be implemented with radiographic guidance.[25] Furthermore, the murine caudal spine consists of 27 intervertebral discs, compared to just 5 in the lumbar spine,[34] and thus enable better control of inter-animal variability by allowing comparisons of IVDs subjected to different treatment conditions

within the same mouse. Therefore, the caudal spine may be more experimentally efficient for investigating IVD-specific disease mechanisms.

To effectively leverage the advantages of the caudal model, it is crucial to define the progression of the inflammatory cascade and pain-related neurovascular features over time. Both neurites and vessels have been observed in aged mouse lumbar IVDs[35] and in human degenerated IVDs[8], but the time course of how the caudal IVD will recapitulate these features is unclear. Therefore, the objective of this study is to define the temporal progression of neurites, vessels, and the IVD's production of chemokines during injury-induced degeneration of the mouse caudal IVD.

2. Materials and Methods

2.1 Animal model

All animal procedures were performed with Washington University School of Medicine IACUC approval. Three-month-old C57BL6/J female mice (N = 35) were used in this study. They were housed under standard animal husbandry conditions (in a temperature-controlled [21□±□1°C] room with normal 12-h light/dark cycles). Bilateral puncture with 30G needle of caudal (Coccygeal - Co) intervertebral discs (IVD) was performed and adjacent IVDs were used as internal controls. Pre- and post-procedural X-ray (Faxitron UltraFocus 100) was used to locate the IVDs of interest and confirm puncture. Co4/5 and Co6/7 were injured with Co3/4 and Co7/8 acting as internal controls. A set of animals (n = 5) underwent a sham procedure to create a superficial injury where the skin and surrounding soft tissue was punctured. Longitudinal assessment of pain behavior and locomotive performance was performed on a subset of animals (Supplemental methods). Mice were euthanized at 2, 4 and 12 weeks (n = 9-10 per timepoint) after injury; all sham mice were taken out to 12 weeks. Paired control and injured IVDs from bilateral puncture mice were divided between OCT embedded histology (Co3/4 and Co4/5; n = 9-10 per timepoint), paraffin embedded histology (Co7/8 and Co6/7; n = 5 per timepoint) and organ culture (Co7/8 and Co6/7; n.= 4-5 per timepoint). Sham control and punctured IVDs were divided between immunohistochemistry (Co3/4 and Co4/5) and paraffin embedded histology (Co7/8 and Co6/7). The lumbar dorsal root ganglions were also extracted from a subset of animals and underwent staining for TRPV1 (Supplemental methods). All samples for histology were immediately fixed in 4% paraformaldehyde at time of sacrifice for 24-48 hours.

2.2 Paraffin embedded histology

Spinal segments with Co7/8 and Co6/7 (n = 5 per timepoint) were embedded in paraffin and 10 μm thick sagittal sections were stained with Safranin-O against FAST green. IVDs were graded using a standardized 35-point histopathology scale.[36] Three independent blinded individuals graded all histological sections to consensus.

2.3 Quantification of Secreted Factors

Co7/8 and Co6/7 (n = 4-5 each per timepoint) functional spinal units (FSUs) were immediately placed in tissue culture media at time of sacrifice. Culture media consisted of 1:1 Dulbecco's modified Eagle's medium: Nutrient mixture F-12 (DMEM:F12) supplemented with 20% fetal bovine serum and 1% penicillin–streptomycin. FSUs were cultured for 6 days at 37°C and 5% CO_2 with a complete media change after 3 days. Day 6 media was collected and analyzed as described here.

Chemokines were measured using the Luminex™ 200 system (Luminex) conducted by Eve Technologies Corp. using two separate kits, a 32-plex and a 12-plex assays (MilliporeSigma) to detect a total of 44 markers. The 32-plex included Eotaxin (CCL11), granulocyte colony-stimulating factor (GCSF), granulocyte-macrophage colony-stimulating factor (GMCSF), IFN-γ, IL-1α, IL-1β, IL-2, IL-3, IL-4, IL-5, IL-6, IL-7, IL-9, IL-10, IL-12 (p40), IL-12 (p70), IL-13, IL-15, IL-17, IP-10 (CXCL10), KC (CXCL1), leukemia inhibitory factor (LIF), LIX (CXCL5), MCP-1 (CCL2), MCSF, MIG (CXCL9), MIP-1α (CCL3), MIP-1β (CCL4), MIP-2 (CXCL2), RANTES (CCL5), TNFα, and VEGFA. The 12-plex measured 6Ckine/Exodus2 (CCL21), Fractalkine (CX3CL1), IFN-β1, IL-11, IL-16, IL-20, MCP-5 (CCL12), MDC (CCL22), MIP-3α (CCL20), MIP-3β (CCL19), TARC (CCL17), and TIMP-1. Assay sensitivities of these markers range from 0.3–30.6 pg/mL.

Matrix metalloproteases (MMPs) were quantified using a single 5-plex kit (MilliporeSigma). This kit measured MMP-2, MMP-3, MMP-8, proMMP-9 and MMP-12. Assay sensitivities of these markers range from 1.6 – 8.4 pg/mL. Individual analyte sensitivity values for all kits are available in the MilliporeSigma MILLIPLEX® MAP protocol.

2.4 Evaluation of intradiscal vascularization and innervation

Spinal segments including Co3/4 and Co4/5 IVDs (n = 9-10 per timepoint) were embedded in OCT and sectioned along the sagittal plane at a 50 µm thickness. Frozen sections were stained with anti-protein gene product 9.5 (PGP9.5) and anti-endomucin (EMCN) against DAPI. PGP9.5 is a neuronal marker for

sensory and autonomic nerve fibers and EMCN is an endothelial cell marker. Visualization of PGP9.5 and EMCN was achieved with Alexa Fluor 488 (green) and Alexa Fluor 647 (red) antibodies, respectively.

Three-dimensional image stacks were obtained via confocal fluorescence microscopy (DMi8, Leica Microsystems) and a maximum intensity image of each 50 μm section was generated for analysis. Nerves and vessels were semi-automatically traced using ImageJ 2.3.0 SNT plugin.[37] Individual structure lengths were tabulated and total neurite and vessel length was calculated including both the posterior and anterior sides of the IVD. The outer annulus fibrosus and immediately adjacent tissues were included as the region of interest (ROI) for quantification.

2.6 Statistics

A paired two-way ANOVA was used to test for an effect of injury and week post-injury between the experimental and control segments, at a significance level of 0.05 with a post hoc Turkey HSD (Prism 10.2.2, GraphPad). A paired t-test was used to test for an effect of the superficial injury on experimental levels versus control segments in the sham-injured group only (12 weeks).

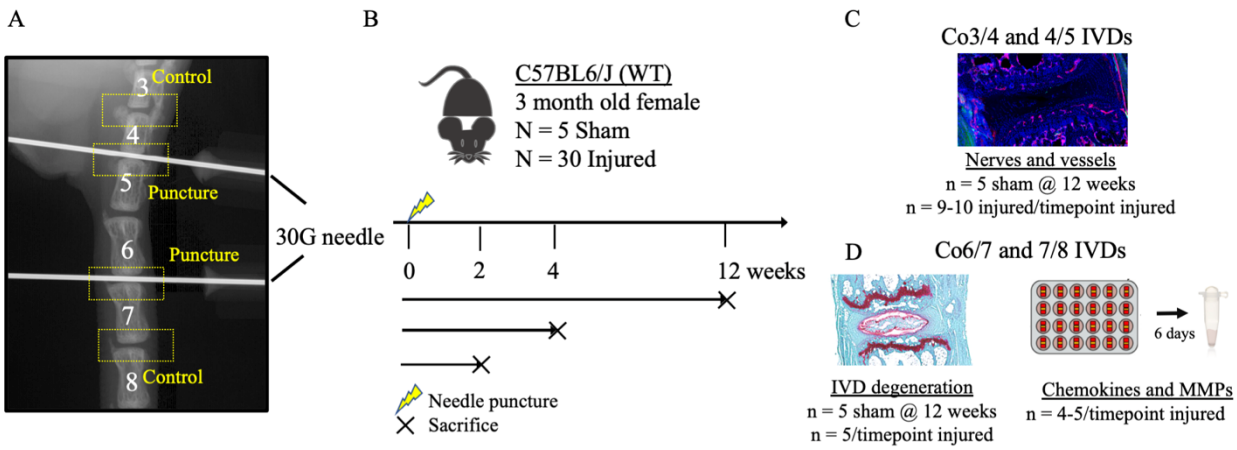

Figure 1: Bilateral caudal injury model in female C57BL6/J mice. (A) Injury of Co4/5 and Co6/7 IVDs were confirmed via X-ray. The Co3/4 and Co7/8 IVDs were used as internal controls within the same animal. (B) Bilateral puncture mice were sacrificed at 2, 4 and 12 weeks post injury while all Sham mice were sacrificed at 12 weeks. Sham was a superficial injury limited to the skin and surrounding tissue. The internal controls (Co3/4 and 7/8) and injured (Co4/5 and 6/7) IVDs were divided between (C) Immunohistochemistry for nerves (Green: protein gene product 9.5; PGP9.5) and vessels (Red: endomucin; EMCN) stained against DAPI (Blue) and (D) Safranin-O against FAST Green staining for IVD degeneration and tissue culture for IVD-specific chemokine and MMP production.

Results

3.1 Direct injury to the intervertebral disc causes rapid and sustained degeneration

Bilateral puncture of the caudal intervertebral disc (IVD) resulted in mild to severe IVD degeneration (Fig 2A). Complete collapse of the IVD was observed in the most severe cases. The control IVDs shown are from the same animal that exhibited the most severe degeneration. Co6/7 and Co7/8 IVDs from sham and bilateral puncture mice were graded on a histopathologic scale for IVD degeneration and total IVD grade was significantly increased in punctured IVDs compared to internal controls of injured ($p<0.05$, ANOVA) but no differences were detected in these levels in the sham mice ($p=0.1$, t-test; Fig. 2B). Multiple compartments of the IVD showed degenerative changes, including the nucleus pulposus, annulus fibrosus and the interfaces at all timepoints after injury while cartilaginous endplates were only significantly degenerated at 12 weeks following injury (Fig. 2C). No effect of injury was observed in any pain behavior or locomotive assessments (Supplemental results).

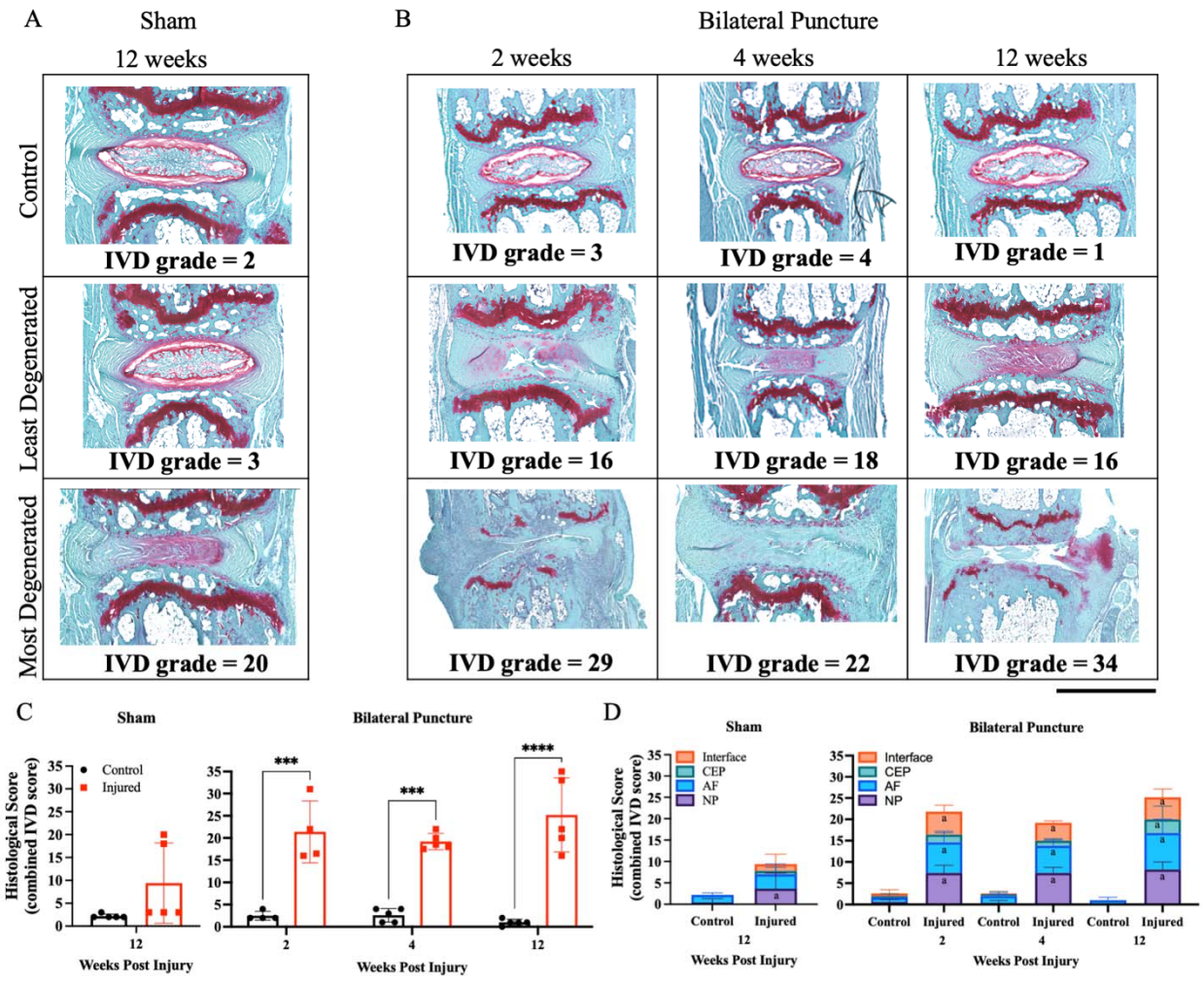

Figure 2: IVD degeneration is quick and sustained following bilateral puncture of the caudal IVD. Representative Safranin-O stained sections of a representative control and the least and most degenerated injured IVD from (A) sham and (B) bilateral puncture mice at 2, 4 and 12 weeks. Histopathological grading of IVD degeneration ranges from moderate to severe with collapse of the IVD following puncture. (C) Total degenerative grade was significantly increased at 2, 4 and 12 weeks after injury compared to internal control which was not seen in sham. (D) Compartmentalized difference in degeneration between control and stab IVDs was seen in the nucleus pulposus, annulus fibrosus and at the interfaces (a indicates $p < 0.05$ compared to internal controls). Data (A and B) were statistically analyzed via paired two-way ANOVA with post-hoc Turkey HSD for control vs. injured. * indicates $p < 0.05$. ** indicates $p < 0.01$; **** indicates $p < 0.001$ in posthoc comparison. Scale bar is 500 µm.

3.2 Chemokine production peaks at 2 weeks after injury

Forty-four distinct chemokines and five MMPs were measured from the culture media of control and punctured functional spinal units from injured mice. An effect of injury was seen in both pro-inflammatory chemokines (IL6 and TNFα) and immune cell recruitment chemokines (CCL4, CCL12, CCL17, CCL20, CCL21, CCL22 and CXCL2) (Fig 3). TNFα and IL1β are pivotal inflammatory chemokines in IVD degeneration, and in this experimental model we only see increased TNFα expression.[38,39] The greatest difference between injured and control IVDs in chemokine production occurred 2 weeks after injury where significantly higher expression of CCL12, CCL17, CCL20, CCL22 and TNFα with all but CCL20 returning to control levels by 4 weeks post injury and CCL20 by 12 weeks post injury (Fig 3A-E). CCL21 was elevated at 12 weeks after injury (Fig 3G). MMP-2 was detected as being affected by injury with the peak at 12 weeks post injury (Fig. 3J).

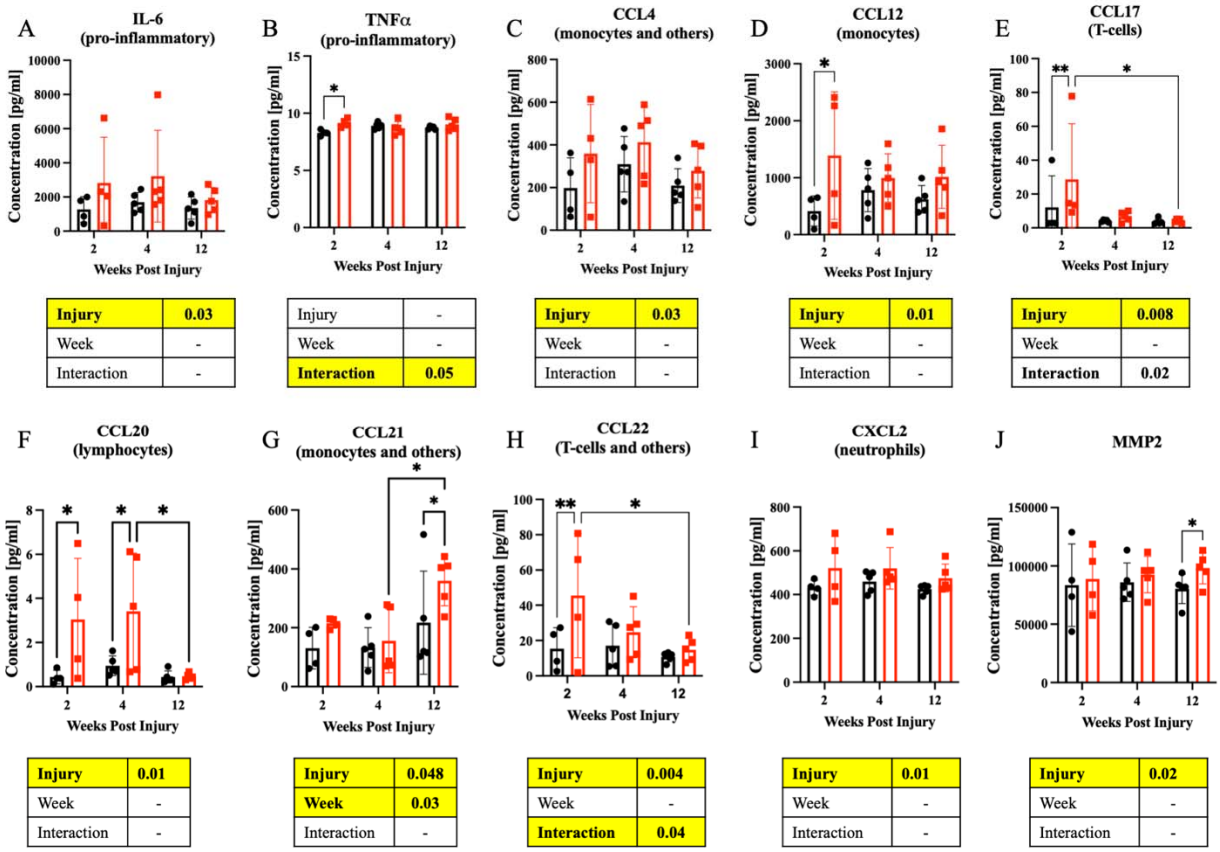

Figure 3: The injured IVD increased chemokine and MMP production. Chemokines measured can broadly be characterized into 2 categories: pro-inflammatory and immune cell recruitment. Pro-inflammatory chemokines (A) IL-6 appears chronically elevated with injury while (B) TNF□ peaks at 2 weeks following injury. Immune cell recruitment chemokines are further categorized by their canonical functions. There were also increases in chemokines associated with monocytes, (C) CCL4, (D) CCL12 and (G) CCL21, with T-cells, (E) CCL17 and (H) CCL22 and lastly, (F) CCL20 which signals to lymphocytes and (I) CXCL2 to neutrophils. (J) MMP-2 was the only of the five MMPs measured that was elevated with injury. * indicates $p < 0.05$. ** indicates $p < 0.01$; **** indicates $p < 0.001$ in posthoc comparison.

3.3 Innervation and vascularization propagate at different temporal trajectories

PGP9.5+ neurite and EMCN+ vasculature structures were manually segmented on a maximum projection image (Fig 4A). The region of interest (ROI) contained the anterior and posterior outer annulus fibrosus and surrounding tissue. High magnification ROIs show innervation and vascularization that colocalize in these areas (Fig 4B). Nerve and vessel structures were semi-automatically traced and lengths were tabulated in each IVD.

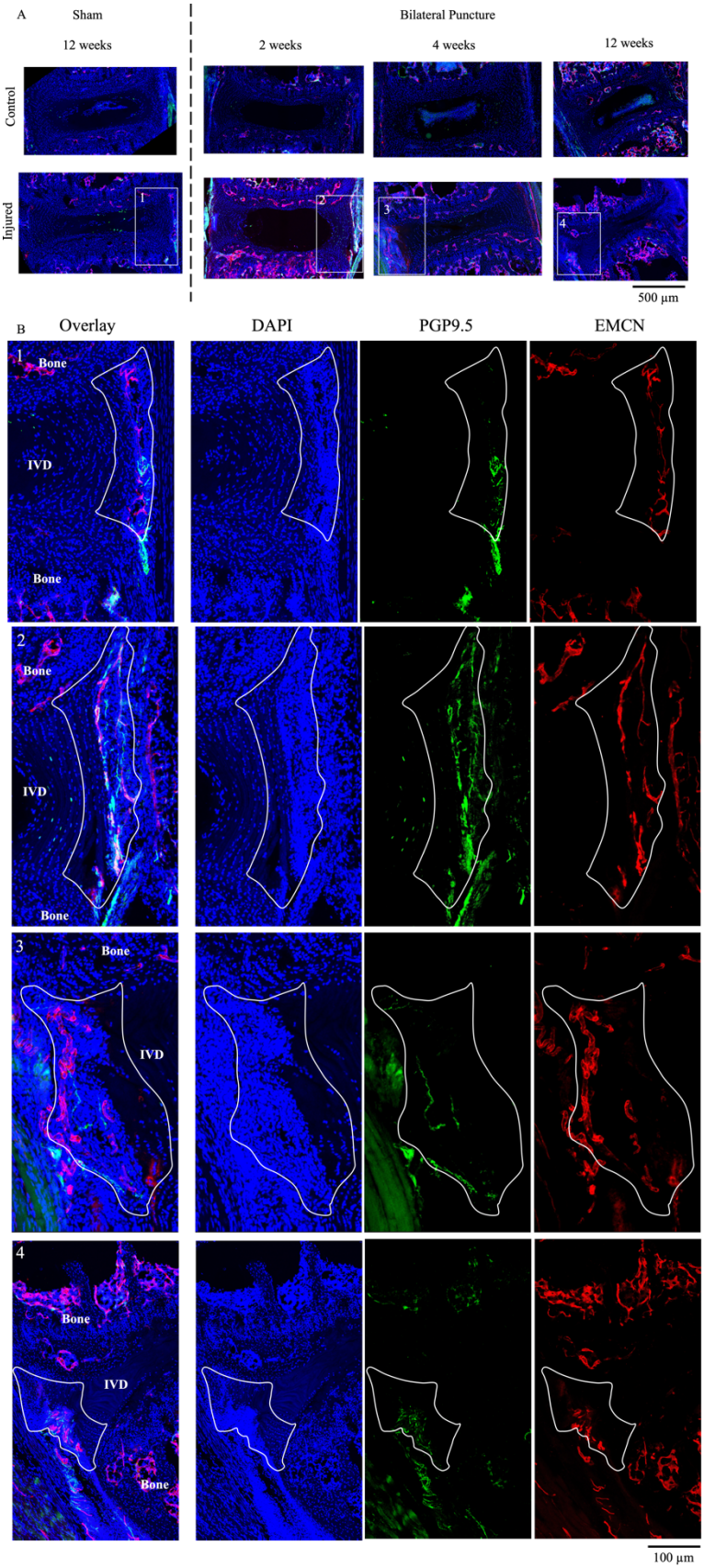

Figure 4: Representative images showing infiltration of neurites and vessels. (A) Maximum projection immunofluorescence images stained with PGP9.5 (Green) and EMCN (Red) against DAPI (blue) from sham and bilateral puncture mice. Control and injured are paired samples. Both the medial and lateral sides of the IVD are semi-automatically traced in ImageJ and used for further analysis. (B) Zoomed in regions from injured IVDs (sham and bilateral puncture). ROI, circled in white, includes the outer annulus fibrous (infiltrating and on the periphery) and surrounding disorganized tissue.

Sham mice showed negligible amounts of innervation and vascularization within their IVDs. Total length of each feature in each IVD was measured and an increased presence of both structures was observed as early as 2 weeks after injury (Fig 5A-B). PGP9.5+ neurite structures are observed 2 weeks following injury and remain consistently increased through the 12 week period; in comparison, EMCN+ vessels peak at 4 weeks and appear to recede by 12 weeks after injury. Violin plots of punctured IVDs from injured mice show the tabulation of individual nerve and vessel lengths that were measured with the total number of structures written above the plot (Fig 5C-D). The distribution of nerves remains consistent through all 12 weeks while the number of vessels in the 150-300 μm range is dramatically reduced at 12 weeks compared to 4 weeks post injury.

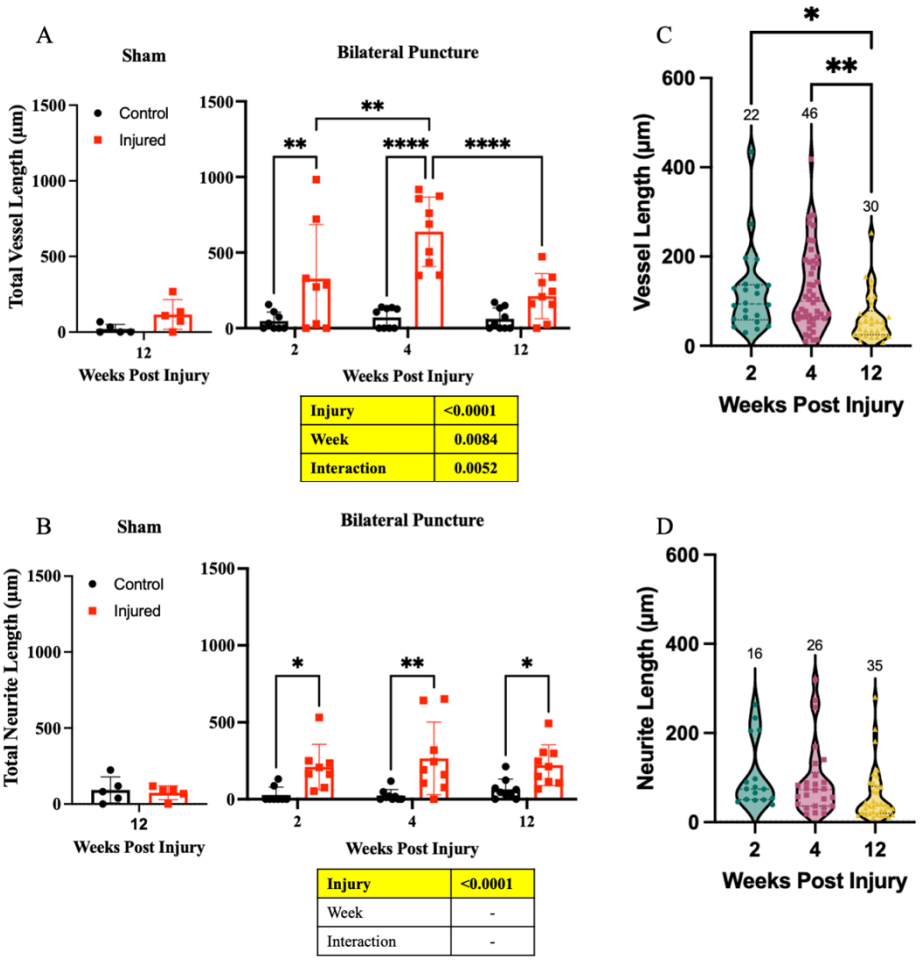

Injury	<0.0001
Week	0.0084
Interaction	0.0052

Injury	<0.0001
Week	-
Interaction	-

Figure 5: Quantification of feature lengths reveal divergent temporal progression of vessels and neurites. All individual vessels and neurites were semi-automatically traced and their lengths tabulated. Total length (sum of all individual lengths) of (A) vessels and (B) nerves demonstrate the presence of both structures as early as 2 weeks after injury. Infiltrating vessels peak at 4 weeks and recede out to 12 weeks after injury compared to nerves which remain consistently present through all 12 weeks. Violin plots of the bilateral punctured IVDs of (C) vessel and (D) nerve length seems to demonstrate that the decreased total vessel length is mainly due to a reduced number of longer vessels compared to both 2 and 4 weeks after injury. Number of vessels/nerves traced is indicated above each violin plot. * indicates $p < 0.05$. ** indicates $p < 0.01$; **** indicates $p < 0.001$ in posthoc comparison.

Discussion

IVD injury models are a commonly utilized tool for studying the progression of IVD degeneration. In contrast to the lumbar spine, where degeneration is known to evoke changes in pain behavior[24,40], we did not observe any behavioral changes following injury in the caudal spine (Fig. S1). Thus, the caudal IVD injury model is perhaps best suited to evaluate IVD-specific responses during degeneration. The advantage of a non-invasive surgical approach and access to multiple levels promotes the reduction in number of research animals used in accordance to the 3R principle.[41] The use of the caudal spine also minimizes the interference due to the disruption and inflammation of surrounding tissues compared to the complex surgical access to the lumbar spine. While there have been extensive studies showing the structural and compositional degenerative changes following caudal puncture[25,29,30,42,43], limited data exists on additional aspects of IVD degeneration including innervation[27,28] and vascularization and chemokine secretion from the explanted IVD.[44]

Bilateral puncture of the caudal IVD resulted in quick and sustained IVD degeneration up to 12 weeks post-injury. Both proinflammatory (IL6 and TNFα) and chemokines (CCL4, CCL12, CCL17, CCL20, CCL21, CCL22 and CXCL2) were elevated with injury, with the highest expression of a subset of chemokines compared to controls at 2 weeks following injury. These chemokines canonically recruit monocytes, T-cells, and lymphocytes (Fig.3).[45] Yet chemokines are known to be pleiotropic and have been associated with additional functions such as IVD degeneration, pain, neurite growth and angiogenesis.[46] For example, CCL4 has been shown to be elevated in degenerated human IVDs and associated with pain behavioral changes in a rat model of IVD degeneration.[6,47,48] TNFα injected into rat lumbar IVDs has been shown to enhance pain behavior changes, possibly through irritation of nerve endings.[33] CCL17 and CCL21 induced dorsal root ganglion (DRG) axonal growth [49,50] and CXCL2 is a known mediator of angiogenesis.[51] CCL17 and CCL22 through the receptor CCR4 were indicated to play a role in pain development and CCL22 was able to activate neurons and increase neuron excitability.[52] Chemokines production of the IVD following injury may help provide further insights into the

pathoanatomy of innervation and vascularization as well as provide possible pathways for IVD degeneration associated low back pain.

Innervation of the IVD may be the potentiator of low back pain observed with lumbar puncture models and this feature is recapitulated here in the caudal spine. Studies have previously illustrated innervation of the IVD following injury with detection of PGP9.5+ or CGRP+ staining injured IVDs, but without any quantification of the structures.[19,26,28] Further, the coincidence of vascularization with neo-innervation has been previously observed but the time course of vessel propagation into the IVD following injury has not been documented. To address these previous limitations, we semi-automatically traced neurite and vascular structures on maximum projection images of PGP9.5 and EMCN stained thick sections.[37] This allowed for the tabulation of neurites and vessels present in the region of interest and their lengths for comparison where we saw a time-dependent vessel but not neurite infiltration of the outer annulus fibrosus and surrounding tissue. Penetration of the IVD by vessels would be considered prerequisite to infiltration by circulating cells, including monocytes and other immune cells that might be responsible for secretion of the chemokines.

Behavioral assays can be used following lumbar puncture to quantify pain.[20,23,24,26] A limitation of the caudal puncture model is that we do not expect to see behavioral changes that would be traditionally associated with low back pain. No differences in behavioral measures between sham and bilateral puncture mice were detected (Fig. S1). Alternative measures of pain can include sensitization of the tail to mechanical and thermal stimuli (e.g., Hargreave's test, tail-flick).[28,53] Another possible surrogate of pain-related change is to quantify molecular expression of neurotrophic factors in the innervating lumbar dorsal root ganglia (DRG). The DRG has been linked to chronic pain, and the increase in the expression of pain-related neuropeptides as well as neuronal excitability may be the mediators of discogenic pain.[54] Ongoing work utilizes immunohistochemical staining for altered presence of neurotrophic factors in lumbar DRGs that have a demonstrated role in mediating pain transmission in the spine such as transient receptor potential cation channel subfamily V member 1 (TRPV1) (Fig. S2).

In this study we used utilized a more sophisticated method to quantify innervation and vascularization of the IVD than has been previously done in puncture models. Protein analysis the IVD secreted chemokines revealed potential molecular mediators of IVD degeneration, innervation and vascularization with relevance to generation of inflammation and pain. Many of the secreted chemokines found to be elevated may be associated with increased presence of infiltrating monocytes that may include macrophages, B-cells or T-cells.[55,56] Not surprisingly, the key angiogenic factor, VEGFA, was not elevated at any of the measured timepoints. VEGFA is critically expressed early following tissue repair promote early angiogenesis, [55] and by two-weeks following injury VEGFA has already exerted its effects as evidenced by robust vessel formation. In this study, we are limited to chemokines differentially expressed between the injured and control IVDs; thereby, excluding chemokines that are more systemically expressed following puncture. Recent work shows that the chronic NFκB activation in the caudal IVD produces a secretome that promote macrophage migration.[57] Our data here confirm that a degeneration-causing injury will upregulate a plethora of chemokines that will likely recruit multiple immune cell types[55], concomitant with increasing neurovascular features. Future studies quantifying the presence of these immune cells would advance our understanding of a role for local versus systemic changes in modulating chemokine secretion, as well as key factors that govern the infiltration of these pain-associated features.

Acknowledgements

We gratefully acknowledge the support of the Washington University Musculoskeletal Research Center. Multiplex Luminex cytokine panels were analyzed by Eve Technologies Corp.

Funding

This work was conducted with funding support from National Institute of Health: R01AR074441, R01AR077678, R21AR081517, T32 DK108742, and P30AR074992.

Literature Cited

1. Hoy D, March L, Brooks P, et al. The global burden of low back pain: estimates from the Global Burden of Disease 2010 study. *Ann Rheum Dis*. 2014;73(6):968-974. doi:10.1136/ANNRHEUMDIS-2013-204428

2. Luoma K, Riihimäki H, Luukkonen R, Raininko R, Viikari-Juntura E, Lamminen A. Low back pain in relation to lumbar disc degeneration. *Spine (Phila Pa 1976)*. 2000;25(4):487-492. doi:10.1097/00007632-200002150-00016

3. Hoy D, Bain C, Williams G, et al. A systematic review of the global prevalence of low back pain. *Arthritis Rheum*. 2012;64(6):2028-2037. doi:10.1002/ART.34347

4. Zehra U, Tryfonidou M, Iatridis JC, Illien-Jünger S, Mwale F, Samartzis D. Mechanisms and clinical implications of intervertebral disc calcification. *Nat Rev Rheumatol*. 2022;18(6):352. doi:10.1038/S41584-022-00783-7

5. Phillips KLE, Chiverton N, Michael ALR, et al. The cytokine and chemokine expression profile of nucleus pulposus cells: Implications for degeneration and regeneration of the intervertebral disc. *Arthritis Res Ther*. 2013;15(6):1-15. doi:10.1186/AR4408/FIGURES/8

6. Risbud M V., Shapiro IM. Role of cytokines in intervertebral disc degeneration: pain and disc content. *Nat Rev Rheumatol 2013 101*. 2013;10(1):44-56. doi:10.1038/nrrheum.2013.160

7. Lama P, Le Maitre CL, Harding IJ, Dolan P, Adams MA. Nerves and blood vessels in degenerated intervertebral discs are confined to physically disrupted tissue. *J Anat*. 2018;233(1):86. doi:10.1111/JOA.12817

8. Binch ALA, Cole AA, Breakwell LM, et al. Nerves are more abundant than blood vessels in the degenerate human intervertebral disc. *Arthritis Res Ther*. 2015;17(1). doi:10.1186/S13075-015-0889-6

9. Silva MJ, Holguin N. Aging aggravates intervertebral disc degeneration by regulating transcription factors toward chondrogenesis. *FASEB J*. 2020;34(2):1970-1982. doi:10.1096/FJ.201902109R

10. Le Maitre CL, Hoyland JA, Freemont AJ. Catabolic cytokine expression in degenerate and

herniated human intervertebral discs: IL-1β and TNFα expression profile. *Arthritis Res Ther*. 2007;9(4):1-11. doi:10.1186/AR2275/FIGURES/3

11. Kikuchi T, Nakamura T, Ikeda T, Ogata H, Takagi K. Monocyte chemoattractant protein-1 in the intervertebral disc. A histologic experimental model. *Spine (Phila Pa 1976)*. 1998;23(10):1091-1099. doi:10.1097/00007632-199805150-00003

12. Haro H, Shinomiya K, Komori H, et al. Upregulated expression of chemokines in herniated nucleus pulposus resorption. *Spine (Phila Pa 1976)*. 1996;21(14):1647-1652. doi:10.1097/00007632-199607150-00006

13. Bohaud C, Johansen MD, Jorgensen C, Kremer L, Ipseiz N, Djouad F. The Role of Macrophages During Mammalian Tissue Remodeling and Regeneration Under Infectious and Non-Infectious Conditions. *Front Immunol*. 2021;12. doi:10.3389/FIMMU.2021.707856

14. Burke JG, Watson RWG, McCormack D, Dowling FE, Walsh MG, Fitzpatrick JM. Intervertebral discs which cause low back pain secrete high levels of proinflammatory mediators. *J Bone Joint Surg Br*. 2002;84(2):196-201. doi:10.1302/0301-620X.84B2.12511

15. Easson GWD, Savadipour A, Gonzalez C, Guilak F, Tang SY. TRPV4 differentially controls inflammatory cytokine networks during static and dynamic compression of the intervertebral disc. *JOR spine*. 2023;6(4). doi:10.1002/JSP2.1282

16. Easson GWD, Savadipour A, Anandarajah A, et al. Modulation of TRPV4 protects against degeneration induced by sustained loading and promotes matrix synthesis in the intervertebral disc. *FASEB J*. 2023;37(2):e22714. doi:10.1096/FJ.202201388R

17. Paul CPL, Schoorl T, Zuiderbaan HA, et al. Dynamic and static overloading induce early degenerative processes in caprine lumbar intervertebral discs. *PLoS One*. 2013;8(4). doi:10.1371/JOURNAL.PONE.0062411

18. MacLean JJ, Lee CR, Grad S, Ito K, Alini M, Iatridis JC. Effects of immobilization and dynamic compression on intervertebral disc cell gene expression in vivo. *Spine (Phila Pa 1976)*. 2003;28(10):973-981. doi:10.1097/01.BRS.0000061985.15849.A9

19. Lee S, Millecamps M, Foster DZ, Stone LS. Long-term histological analysis of innervation and macrophage infiltration in a mouse model of intervertebral disc injury–induced low back pain. *J Orthop Res*. 2020;38(6):1238-1247. doi:10.1002/JOR.24560

20. Millecamps M, Lee S, Foster DZ, Stone LS. Disc degeneration spreads: long-term behavioural, histologic and radiologic consequences of a single-level disc injury in active and sedentary mice. *Eur Spine J*. 2021;30(8):2238-2246. doi:10.1007/S00586-021-06893-2/FIGURES/3

21. Liu JW, Abraham AC, Tang SY. The high-throughput phenotyping of the viscoelastic behavior of whole mouse intervertebral discs using a novel method of dynamic mechanical testing. *J Biomech*. 2015;48(10):2189-2194. doi:10.1016/j.jbiomech.2015.04.040

22. Walk RE, Moon HJ, Tang SY, Gupta MC. Contrast-enhanced microCT evaluation of degeneration following partial and full width injuries to the mouse lumbar intervertebral disc. *Sci Rep*. 2022;12(1). doi:10.1038/S41598-022-19487-9

23. Qiu S, Shi C, Anbazhagan AN, et al. Absence of VEGFR-1/Flt-1 signaling pathway in mice results in insensitivity to discogenic low back pain in an established disc injury mouse model. *J Cell Physiol*. 2020;235(6):5305. doi:10.1002/JCP.29416

24. Shi C, Das V, Li X, et al. Development of an in vivo mouse model of discogenic low back pain. *J Cell Physiol*. 2018;233(10):6589-6602. doi:10.1002/JCP.26280

25. Tian Z, Ma X, Yasen M, et al. Intervertebral Disc Degeneration in a Percutaneous Mouse Tail Injury Model. *Am J Phys Med Rehabil*. 2018;97(3):170-177. doi:10.1097/PHM.0000000000000818

26. Millecamps M, Stone LS. Delayed onset of persistent discogenic axial and radiating pain after a single-level lumbar intervertebral disc injury in mice. *Pain*. 2018;159(9):1843-1855. doi:10.1097/J.PAIN.0000000000001284

27. Orita S, Ohtori S, Taniguchi A, et al. Direct evidence for sensory innervation of the dorsal portion of the Co5/6 coccygeal intervertebral disc in rats. *Spine (Phila Pa 1976)*. 2010;35(14):1346-1352. doi:10.1097/BRS.0B013E3181C099B0

28. Mohd Isa IL, Abbah SA, Kilcoyne M, et al. Implantation of hyaluronic acid hydrogel prevents the pain phenotype in a rat model of intervertebral disc injury. *Sci Adv*. 2018;4(4). doi:10.1126/SCIADV.AAQ0597/SUPPL_FILE/AAQ0597_SM.PDF

29. Martin JT, Gorth DJ, Beattie EE, Harfe BD, Smith LJ, Elliott DM. Needle puncture injury causes acute and long-term mechanical deficiency in a mouse model of intervertebral disc degeneration. *J Orthop Res*. 2013;31(8):1276-1282. doi:10.1002/JOR.22355

30. Han B, Zhu K, Li FC, et al. A simple disc degeneration model induced by percutaneous needle puncture in the rat tail. *Spine (Phila Pa 1976)*. 2008;33(18):1925-1934. doi:10.1097/BRS.0B013E31817C64A9

31. Xia D, Yan M, Yin X, et al. A Novel Rat Tail Needle Minimally Invasive Puncture Model Using Three-Dimensional Printing for Disk Degeneration and Progressive Osteogenesis Research. *Front Cell Dev Biol*. 2021;9:587399. doi:10.3389/FCELL.2021.587399/BIBTEX

32. Leimer EM, Gayoso MG, Jing L, Tang SY, Gupta MC, Setton LA. Behavioral Compensations and Neuronal Remodeling in a Rodent Model of Chronic Intervertebral Disc Degeneration. *Sci Rep*. 2019;9(1):1-10. doi:10.1038/s41598-019-39657-6

33. Lai A, Moon A, Purmessur D, et al. Annular puncture with tumor necrosis factor-alpha injection enhances painful behavior with disc degeneration in vivo. *Spine J*. 2016;16(3):420-431. doi:10.1016/J.SPINEE.2015.11.019

34. The Anatomy of the Laboratory Mouse. Accessed May 22, 2024. https://www.informatics.jax.org/cookbook/

35. Vincent K, Mohanty S, Pinelli R, et al. Aging of mouse intervertebral disc and association with back pain. *Bone*. 2019;123:246-259. doi:10.1016/j.bone.2019.03.037

36. Melgoza IP, Chenna SS, Tessier S, et al. Development of a standardized histopathology scoring system using machine learning algorithms for intervertebral disc degeneration in the mouse model—An ORS spine section initiative. *JOR Spine*. 2021;4(2):e1164. doi:10.1002/JSP2.1164

37. Arshadi C, Günther U, Eddison M, Harrington KIS, Ferreira TA. SNT: a unifying toolbox for

quantification of neuronal anatomy. *Nat Methods 2021 184*. 2021;18(4):374-377. doi:10.1038/s41592-021-01105-7

38. Johnson ZI, Schoepflin ZR, Choi H, Shapiro IM, Risbud M V. Disc in Flames: Roles of TNF-α and IL-1β in Intervertebral Disc Degeneration. *Eur Cell Mater*. 2015;30:104. doi:10.22203/ECM.V030A08

39. Wang Y, Che M, Xin J, Zheng Z, Li J, Zhang S. The role of IL-1β and TNF-α in intervertebral disc degeneration. *Biomed Pharmacother*. 2020;131. doi:10.1016/J.BIOPHA.2020.110660

40. Olmarker K, Iwabuchi M, Larsson K, Rydevik B. Walking analysis of rats subjected to experimental disc herniation. *Eur Spine J*. 1998;7(5):394. doi:10.1007/S005860050096

41. Tannenbaum J, Bennett BT. Russell and Burch's 3Rs Then and Now: The Need for Clarity in Definition and Purpose. *J Am Assoc Lab Anim Sci*. 2015;54(2):120. Accessed July 12, 2024. /pmc/articles/PMC4382615/

42. Yang F, Leung VYL, Luk KDK, Chan D, Cheung KMC. Injury-induced sequential transformation of notochordal nucleus pulposus to chondrogenic and fibrocartilaginous phenotype in the mouse. *J Pathol*. 2009;218(1):113-121. doi:10.1002/PATH.2519

43. Piazza M, Peck SH, Gullbrand SE, et al. Quantitative MRI correlates with histological grade in a percutaneous needle injury mouse model of disc degeneration. *J Orthop Res*. 2018;36(10):2771-2779. doi:10.1002/JOR.24028

44. Kang JD, Georgescu HI, Mc Lntyre-Larkin L, Stefanovic-Racic M, Evans CH. Herniated cervical intervertebral discs spontaneously produce matrix metalloproteinases, nitric oxide, interleukin-6, and prostaglandin E2. *Spine (Phila Pa 1976)*. 1995;20(22):2373-2378. doi:10.1097/00007632-199511001-00001

45. Sokol CL, Luster AD. The Chemokine System in Innate Immunity. *Cold Spring Harb Perspect Biol*. 2015;7(5):1-20. doi:10.1101/CSHPERSPECT.A016303

46. Dimberg A. Chemokines in Angiogenesis. Published online 2010:59-80. doi:10.1007/82_2010_21

47. Li Z, Liu H, Yang H, et al. Both expression of cytokines and posterior annulus fibrosus rupture are

essential for pain behavior changes induced by degenerative intervertebral disc: An experimental study in rats. *J Orthop Res*. 2014;32(2):262-272. doi:10.1002/JOR.22494

48. Zhang J, Li Z, Chen F, et al. TGF-β1 suppresses CCL3/4 expression through the ERK signaling pathway and inhibits intervertebral disc degeneration and inflammation-related pain in a rat model. *Exp Mol Med*. 2017;49(9). doi:10.1038/EMM.2017.136

49. Urbantat RM, Blank A, Kremenetskaia I, Vajkoczy P, Acker G, Brandenburg S. The CXCL2/IL8/CXCR2 Pathway Is Relevant for Brain Tumor Malignancy and Endothelial Cell Function. *Int J Mol Sci*. 2021;22(5):1-19. doi:10.3390/IJMS22052634

50. Mesquida-Veny F, Hervera A. Neuronal chemokines: new insights into neuronal communication after injury. *Neural Regen Res*. 2023;18(11):2379. doi:10.4103/1673-5374.371352

51. Mehrad B, Keane MP, Strieter RM. Chemokines as mediators of angiogenesis. *Thromb Haemost*. 2007;97(5):755. doi:10.1160/TH07-01-0040

52. Silva JR, Iftinca M, Gomes FIF, et al. Skin-resident dendritic cells mediate postoperative pain via CCR4 on sensory neurons. *Proc Natl Acad Sci U S A*. 2022;119(4). doi:10.1073/PNAS.2118238119/-/DCSUPPLEMENTAL

53. Allen KD, Griffin TM, Rodriguiz RM, et al. Decreased physical function and increased pain sensitivity in mice deficient for type IX collagen. *Arthritis Rheum*. 2009;60(9):2684-2693. doi:10.1002/ART.24783

54. Krames ES. The role of the dorsal root ganglion in the development of neuropathic pain. *Pain Med (United States)*. 2014;15(10):1669-1685. doi:10.1111/pme.12413

55. Clayton SW, Walk RE, Mpofu L, Easson GWD, Tang SY. Analysis of Infiltrating Immune Cells Following Intervertebral Disc Injury Reveals Recruitment of Gamma-Delta (γδ) T cells in Female Mice. *bioRxiv*. Published online March 2, 2024. doi:10.1101/2024.03.01.582950

56. Rohanifar M, Clayton SW, Easson GWD, et al. Single Cell RNA-Sequence Analyses Reveal Uniquely Expressed Genes and Heterogeneous Immune Cell Involvement in the Rat Model of Intervertebral Disc Degeneration. *Appl Sci*. 2022;12(16). doi:10.3390/APP12168244/S1

460 57. Burt KG, Kim MKM, Viola DC, Abraham AC, Chahine NO. Nuclear factor κB overactivation in
461 the intervertebral disc leads to macrophage recruitment and severe disc degeneration. *Sci Adv*.
462 2024;10(23). doi:10.1126/SCIADV.ADJ3194

463

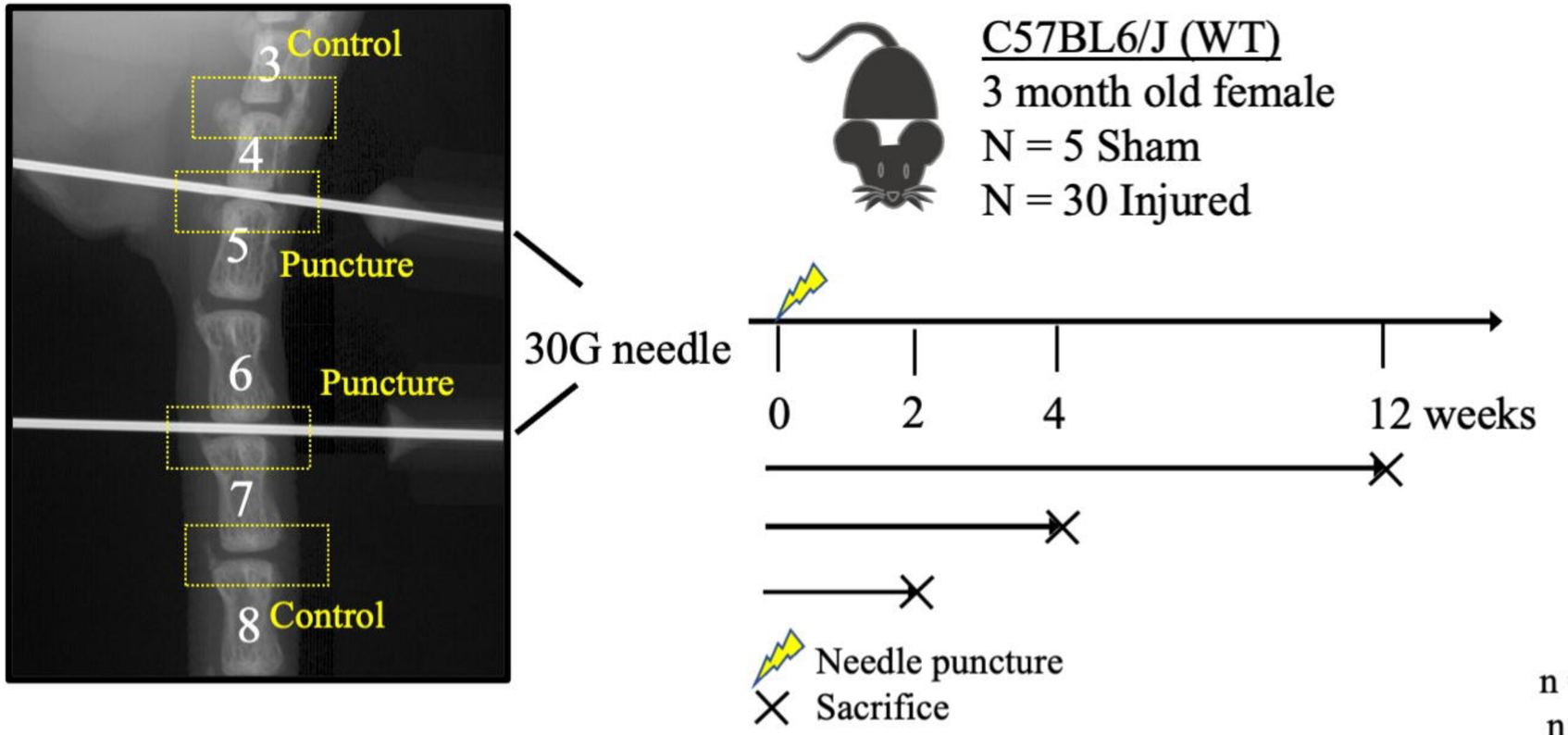
A
3 Control
4
5 Puncture
6 Puncture
7
8 Control
30G needle
B
C57BL6/J (WT)
3 month old female
N = 5 Sham
N = 30 Injured
0
2
4
12 weeks
Needle puncture
Sacrifice
C
Co3/4 and 4/5 IVDs
Nerves and vessels
n = 5 sham @ 12 weeks
n = 9-10 injured/timepoint injured
D
Co6/7 and 7/8 IVDs
6 days
IVD degeneration
n = 5 sham @ 12 weeks
n = 5/timepoint injured
Chemokines and MMPs
n = 4-5/timepoint injured

A

Sham

12 weeks

Control

IVD grade = 2

Least Degenerated

IVD grade = 3

Most Degenerated

IVD grade = 20

B

Bilateral Puncture

2 weeks

IVD grade = 3

IVD grade = 16

IVD grade = 29

4 weeks

IVD grade = 4

IVD grade = 18

IVD grade = 22

12 weeks

IVD grade = 1

IVD grade = 16

IVD grade = 34

C

Sham

Bilateral Puncture

Histological Score (combined IVD score)

Control

Injured

***

***

****

Weeks Post Injury

D

Sham

Bilateral Puncture

Histological Score (combined IVD score)

Interface

CEP

AF

NP

Control

Injured

Weeks Post Injury

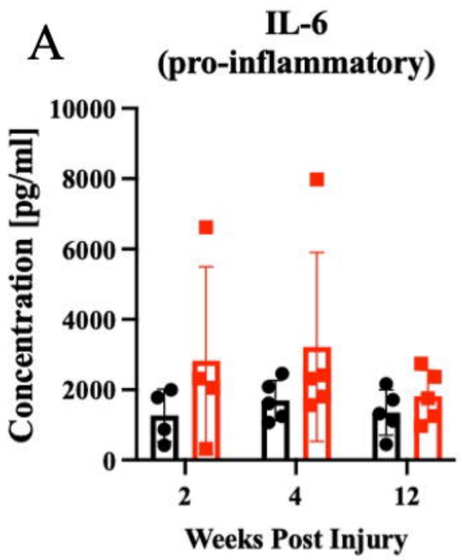

Injury	0.03
Week	-
Interaction	-

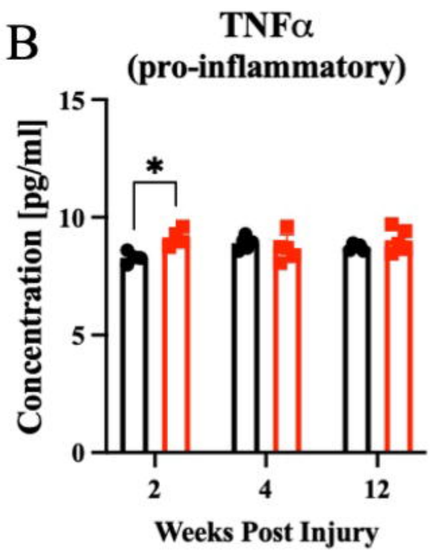

Injury	-
Week	-
Interaction	0.05

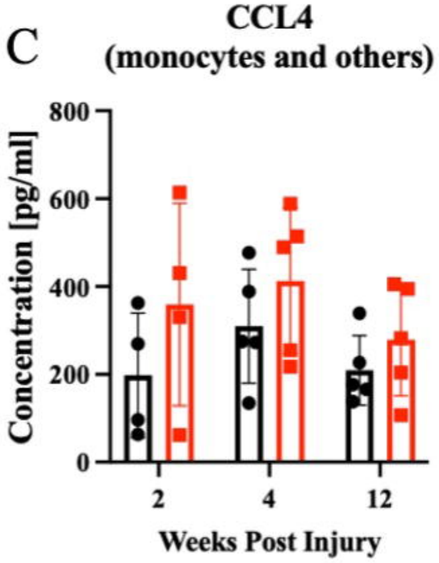

Injury	0.03
Week	-
Interaction	-

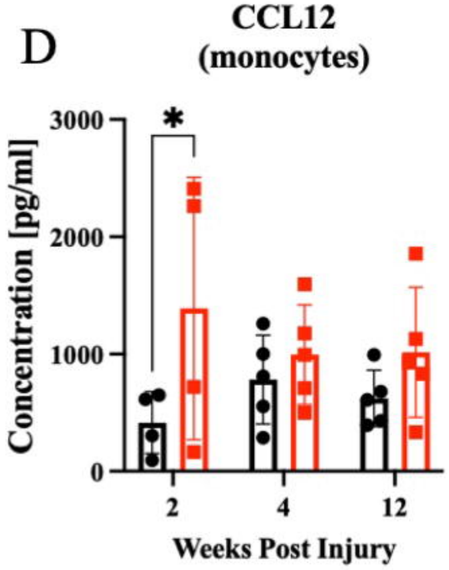

Injury	0.01
Week	-
Interaction	-

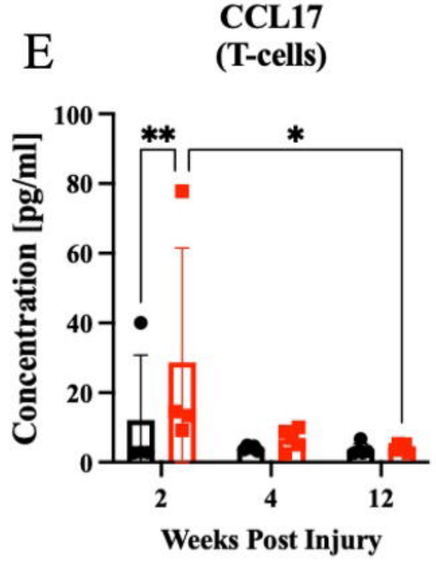

Injury	0.008
Week	-
Interaction	0.02

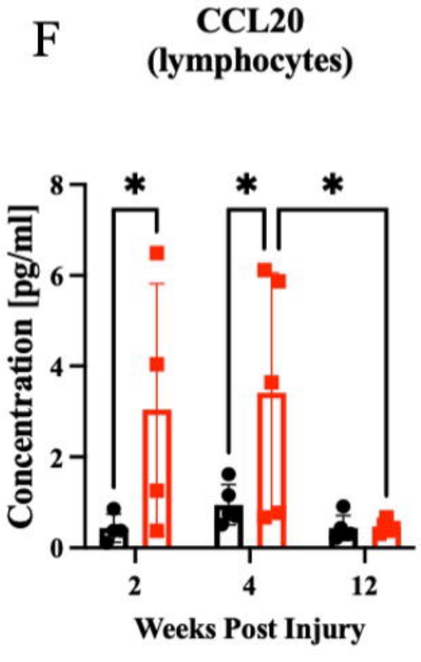

Injury	0.01
Week	-
Interaction	-

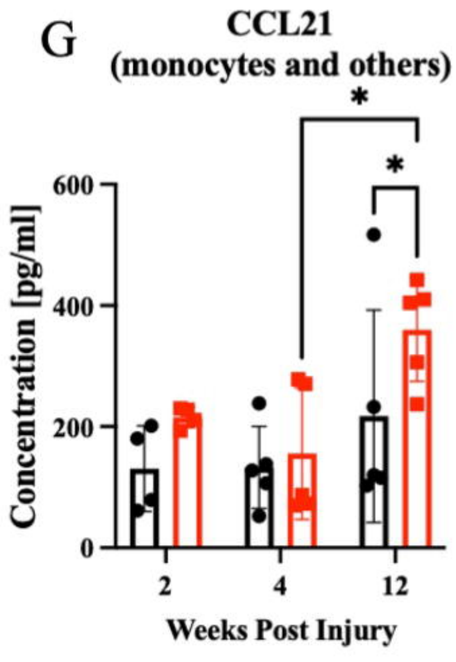

Injury	0.048
Week	0.03
Interaction	-

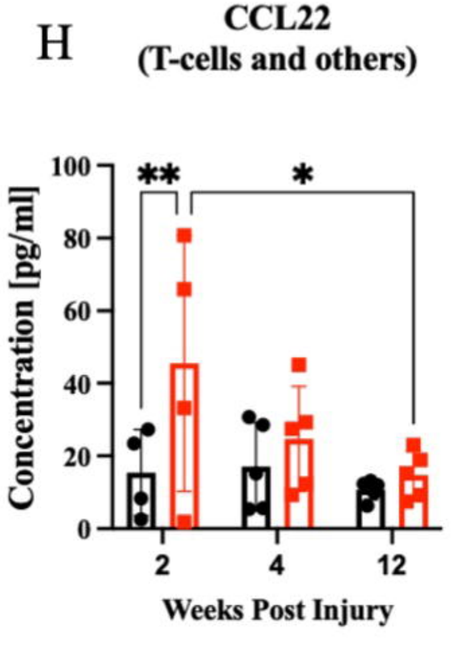

Injury	0.004
Week	-
Interaction	0.04

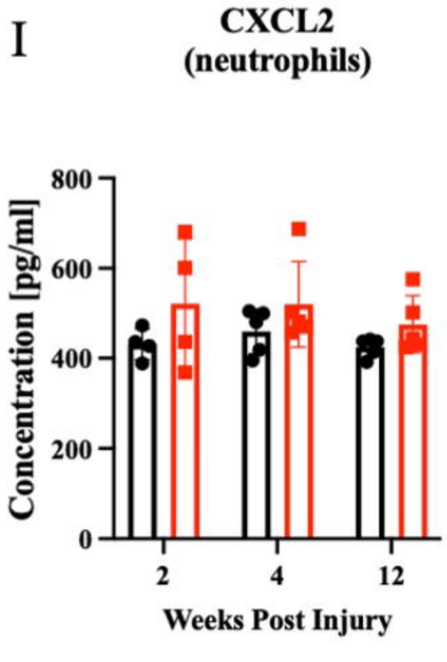

Injury	0.01
Week	-
Interaction	-

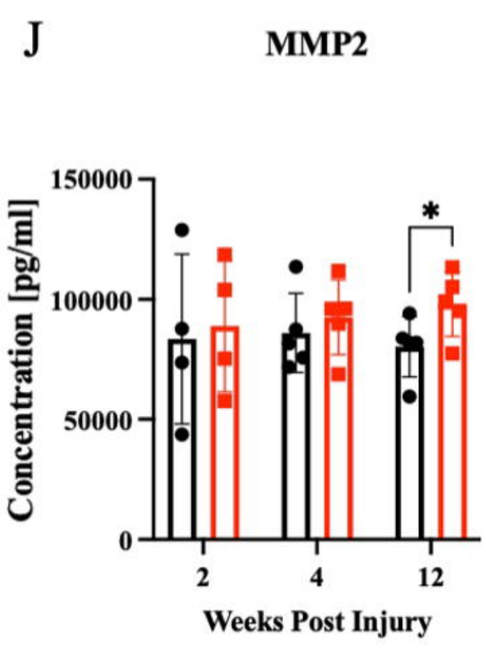

Injury	0.02
Week	-
Interaction	-

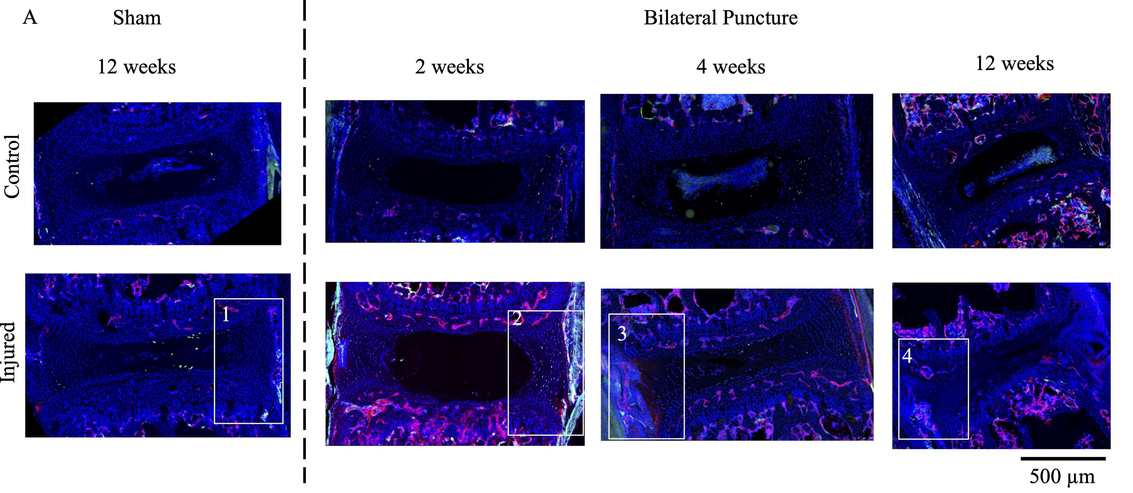
A
Sham
Bilateral Puncture
12 weeks
2 weeks
4 weeks
12 weeks
Control
Injured
1
2
3
4
500 µm

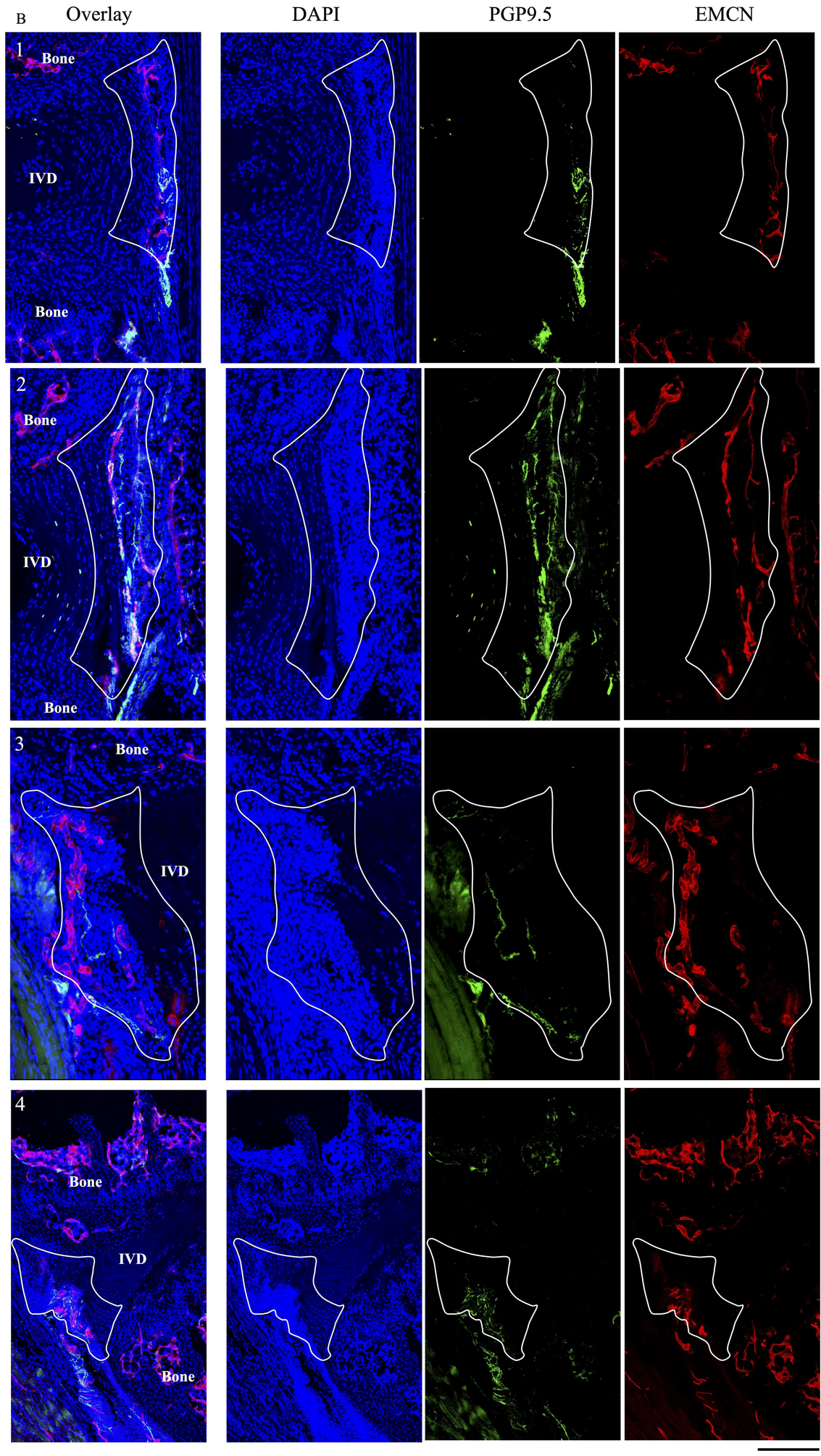
B
Overlay
DAPI
PGP9.5
EMCN
1
Bone
IVD
Bone
2
Bone
IVD
Bone
3
Bone
IVD
4
Bone
IVD
Bone
100 µm

A

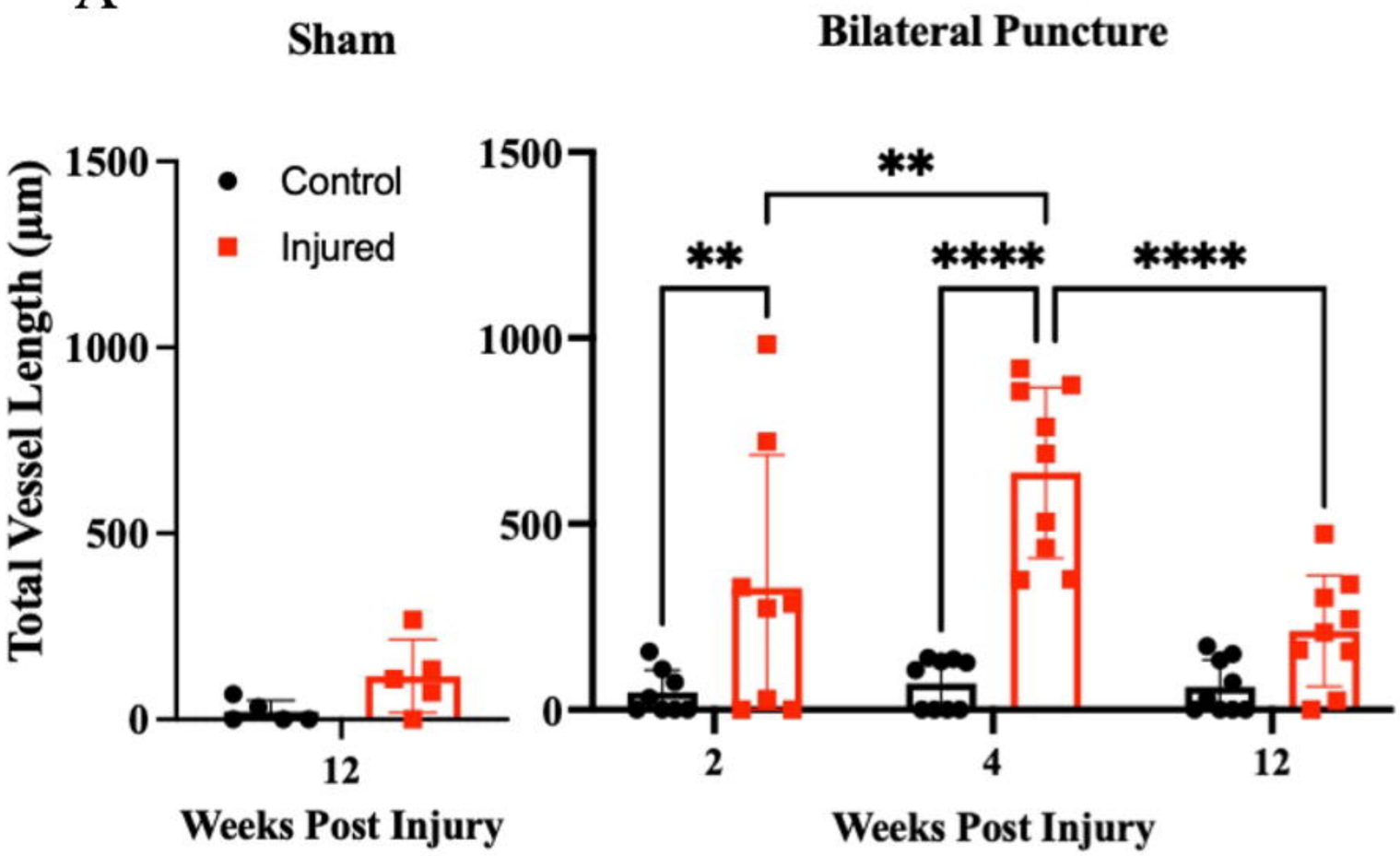

Injury	**<0.0001**
Week	**0.0084**
Interaction	**0.0052**

C

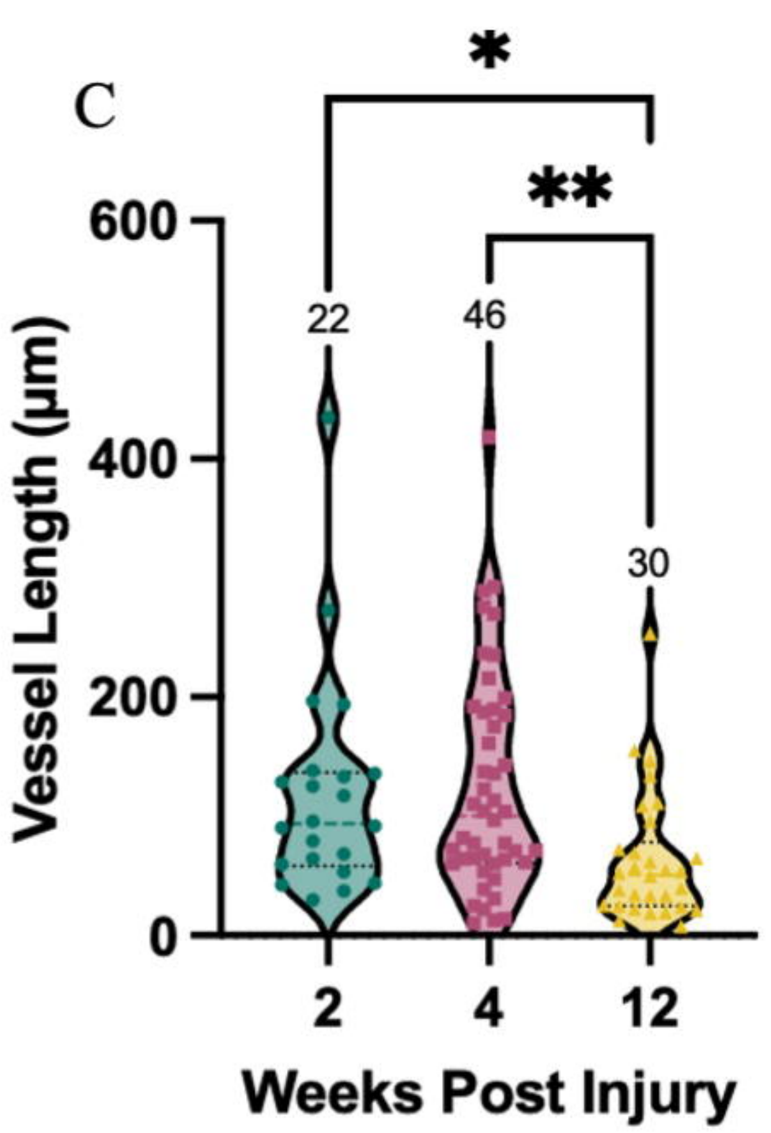

B

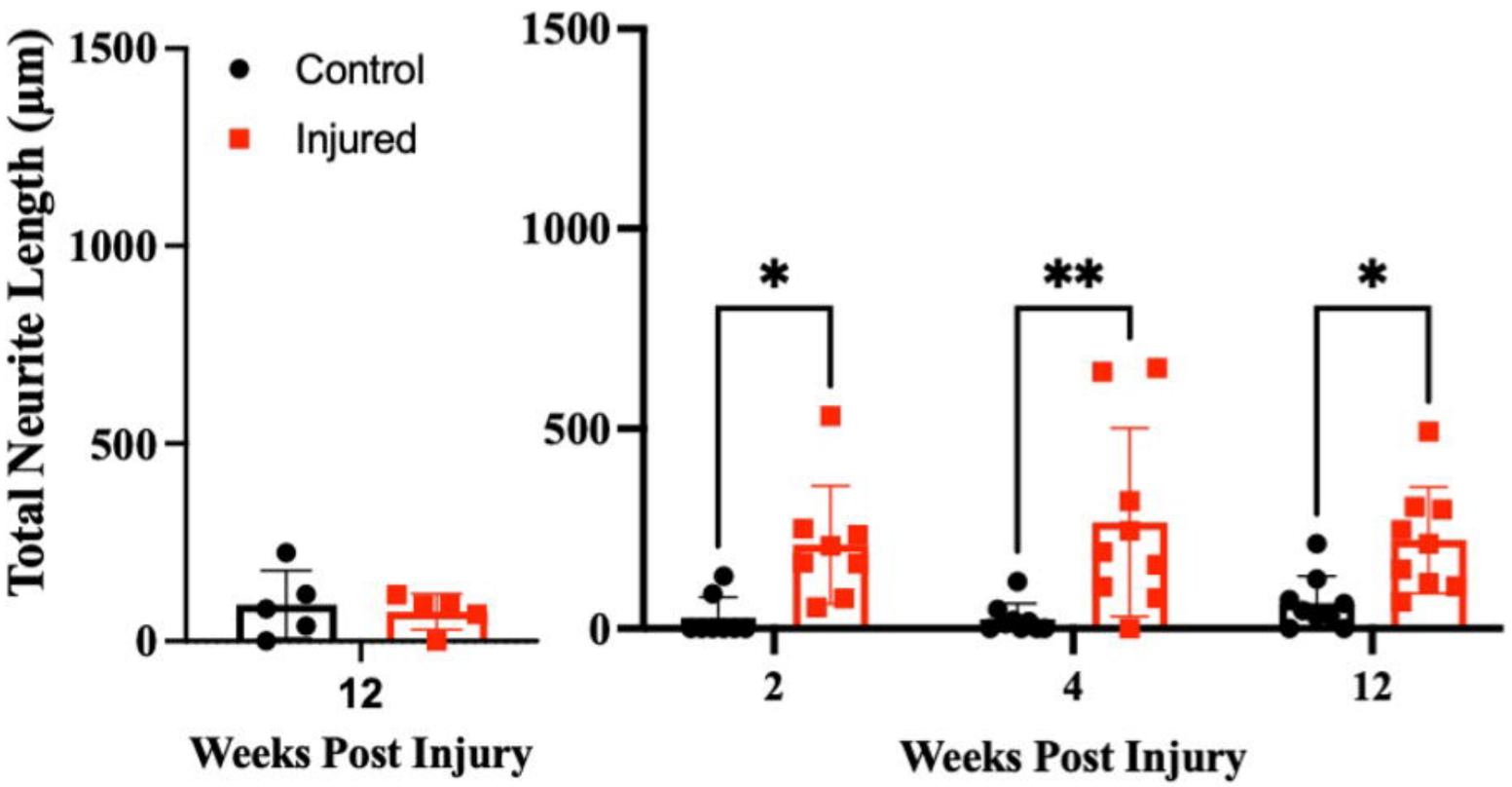

Injury	**<0.0001**
Week	-
Interaction	-

D